Engineering Structures 287 (2023) 116164

Contents lists available at ScienceDirect

Engineering Structures

journal homepage: www.elsevier.com/locate/engstruct

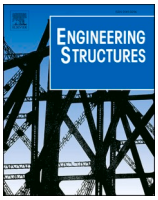

FRP bar-reinforced ultra-high-performance concrete plates with a grouting sleeve connection: Development and flexural behavior

Jun-Jie Zeng [a], Shu-Peng Chen [a], Peng Feng [b], Yan Zhuge [c,*], Kai-Di Peng [d], Jian-Guo Dai [d,*], Tian-Hui Fan [e]

[a] Department of Civil and Transportation Engineering, Guangdong University of Technology, Guangzhou 510006, China
[b] Department of Civil Engineering, Tsinghua University, Beijing 100084, China
[c] UniSA STEM, University of South Australia, South Australia 5095 Australia
[d] Department of Civil and Environmental Engineering, The Hong Kong Polytechnic University, Hong Kong, China
[e] School of Civil Engineering and Transportation, South China University of Technology, Guangzhou, China

ARTICLE INFO

Keywords:
Fiber-reinforced polymer (FRP)
FRP bar
Ultra-high-performance concrete (UHPC)
Grouting sleeve
Flexural behavior

ABSTRACT

Fiber reinforced polymer (FRP) bars have been proposed for use in ultra-high performance concrete (UHPC) as the reinforcement to mitigate/avoid the post-peak strain softening of UHPC under tension and to reduce the fiber dosage used in UHPC. The so-formed FRP-reinforced UHPC plates could be adopted for both structural strengthening and constructing novel structural elements. In this paper, a novel connection based on FRP bars and steel grouting sleeves has been developed for prefabrication construction of FRP bar-reinforced UHPC structures. Flexural tests were conducted to gain understandings of the effects of the connection mode (the staggered connection and the horse tooth connection) and reinforcing fiber type (polyethylene (PE) fibers and steel fibers) in the UHPC on the flexural behavior of connected FRP bar-reinforced-UHPC composite plates. The test results revealed that the proposed connection system is reliable since the composite plates always failed outside the connection zone, and most of the crack opening displacements at the interface of the connection are smaller than 0.2 mm at ultimate. The connection mode and the fiber type had little influence on the first cracking load and the initial bending stiffness of the FRP bar-reinforced UHPC plates, while the horse tooth connection led to a better ductility of the composites plates than the staggered connection mode. At given tolerable deflection of 1/200 span (about 5 mm), the longitudinal strains developed in the CFRP bars were about 2000 με for all specimens.

1. Introduction

The unique merits of ultra-high performance concrete (UHPC), including extraordinary compressive strength and excellent corrosion resistance, have allowed its increasing usage in applications [1–8]. Besides, steel fibers are generally employed to enhance the tensile strength and deformation capacity of UHPC. However, UHPC under tension may exhibit a post-peak strain softening behavior, especially when a low fiber volume fraction is adopted. Strain softening is unexpected because it may lead to some problems such as a localized cracking or brittle failure of the structures. Although increasing fiber dosage could mitigate the strain softening behavior, using excessive fibers in UHPC for enhanced tensile properties may not be a cost-effective approach. On the other hand, the issue of steel fiber corrosion is unavoidable if steel fibers are employed in UHPC.

Fiber-reinforced polymer (FRP) grid has been proposed as internal reinforcement for UHPC to solve the above issues [9–16]. FRP materials (in forms of pultruded sections, grids and rebars) have been widely used in retrofitting of existing RC structures [17–20] and for new designs [21–24]. Existing studies have also indicated that the bond behavior between FRP reinforcement and the cementitious matrix is satisfactory [13–14]. FRP composites also have an excellent tensile strength and satisfactory ultimate tensile strain owning to continuous fibers in FRP composites [25], making FRP-reinforced UHPC composite plates deemed to have excellent tensile properties. Also, FRP reinforcement could alleviate the possible corrosion problem of steel fibers in UHPC. It should be noted that although the fibre corrosion may not be a problem for UHPC structures [3], it is not necessarily meant that the corrosion

* Corresponding authors.
E-mail addresses: jjzeng@gdut.edu.cn (J.-J. Zeng), Yan.zhuge@unisa.edu.au (Y. Zhuge), jian-guo.dai@polyu.edu.hk (J.-G. Dai).

https://doi.org/10.1016/j.engstruct.2023.116164

Available online 26 April 2023

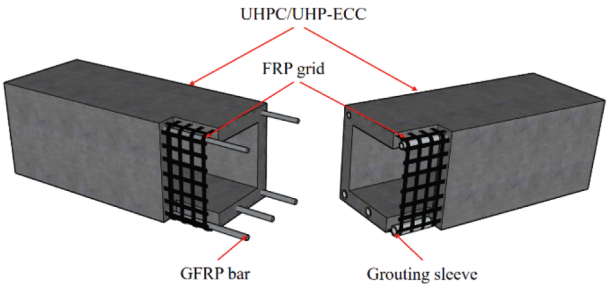

(a) Prefabricated box sections

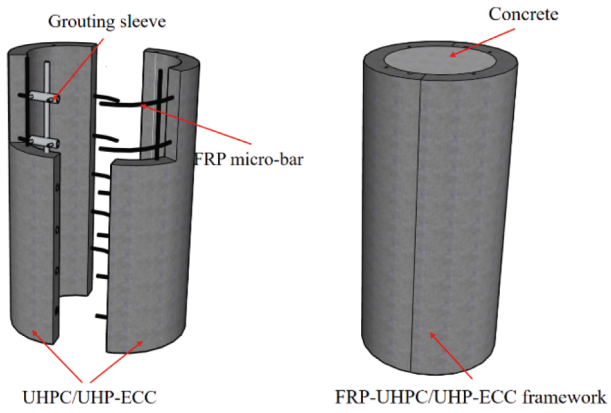

(b) Prefabricated shells for structural strengthening

Fig. 1. Application prospects of FRP-UHPC composite plates.

issue can be avoided. If non-metallic fibers (e.g., polyethylene (PE) fibers) are used in FRP grid-reinforced UHPC composites, problems associated with corrosion are expected to be avoidable and corrosive materials such as fly ash and sea-sand [7] could be directly employed for preparation of UHPC. Capitalizing these advantages, FRP-reinforced UHPC composite plates are promising and could be used for various purposes such as strengthening existing deteriorated structures, developing all kinds of tubular structural members, establishing prefabricated formworks for structures and building marine and offshore structures which require excellent durability. Recently, the authors have proposed using FRP-UHPC plates for developing novel tubular members with prefabrication construction or strengthening existing RC structures (Fig. 1) [8,14,15,27]. Therefore, developing a reliable connection system for the FRP-UHPC plates is of great significance.

Indeed, studies [13–14] have shown that the FRP grid enhanced the ultimate tensile and flexural strengths of UHPC plates by over 200 % and 150 %, respectively. Particularly, the FRP grid reinforced-UHPC composite plates with an FRP reinforcement ratio of about 0.69 % exhibited a tension-stiffening behavior with an ultimate tensile strength of over

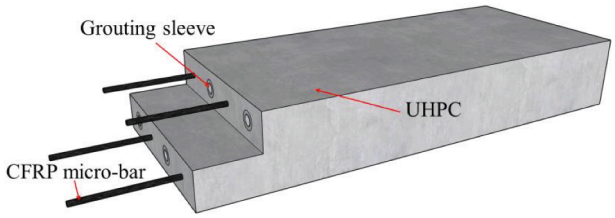

(a) Mode I (staggered connection mode)

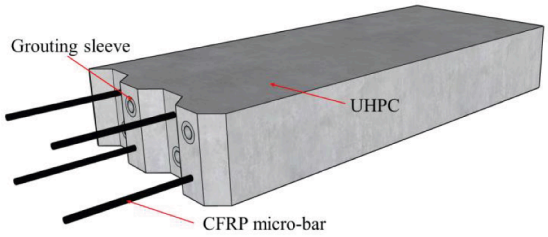

(b) Mode II (horse tooth connection mode)

Fig. 2. Proposed connection system.

25 MPa as well as multiple cracking behaviors [13]. Overall, the presence of FRP grids prevented the load deterioration, and led to a strong tension-stiffening response in the second segment of the load–deflection curves. Meng et al. also found that [12,26] incorporation of FRP grids improved the flexural capacity of UHPC panels by 25 %-54 %, but the flexural capacity of ultra-high-strength mortar (without any fiber reinforcement) panels was not improved. Extensive studies have been conducted on FRP bar reinforced concrete structures [28–33], the existing design codes have specified the connection approach for FRP bars [34–37], and the FRP bars are generally connected by means of lap-spliced connections. Also, connection modes have developed for FRP structures [38–39]. However, to the best of authors' knowledge, no research has been found on connection mode for prefabricated UHPC structural elements reinforced with FRP bars.

Against this background, modes of connection system for FRP reinforced UHPC structures are developed and verified via an experimental program containing eight FRP-reinforced UHPC plates with a grouting sleeve connection subject to bending. Effects of the connection mode (staggered connection and horse tooth connection), fiber type (polyethylene (PE) fibers, and steel fibers) on the flexural behavior of connected FRP bar-reinforced UHPC composite plates are explored. As steel fibers are prone to potential corrosion problems when the UHPC structures are used in a marine environment or other harsh environments, non-metallic fibers polyethylene (PE) fibers are proposed to be used in UHPC.

Table 1
Details of specimens.

Specimen	Length (mm)	Width (mm)	Thickness (mm)	Spacing of the CFRP micro-bar(mm)	Reinforcement ratio of CFRP micro-bar	Connection mode
MI-PE-1,2	1000	220	70	100	0.73 %	I
MI-SF-1,2	1000	220	70	100	0.73 %	I
MII-PE-1,2	1000	220	70	100	0.73 %	II
MII-SF-1,2	1000	220	70	100	0.73 %	II

Note: "M" ——Mode of connection; "PE" —— UHPC with PE fibers; "SF" —— UHPC with steel fibers; Mode I —— Staggered connection; Mode II —— Horse tooth connection.

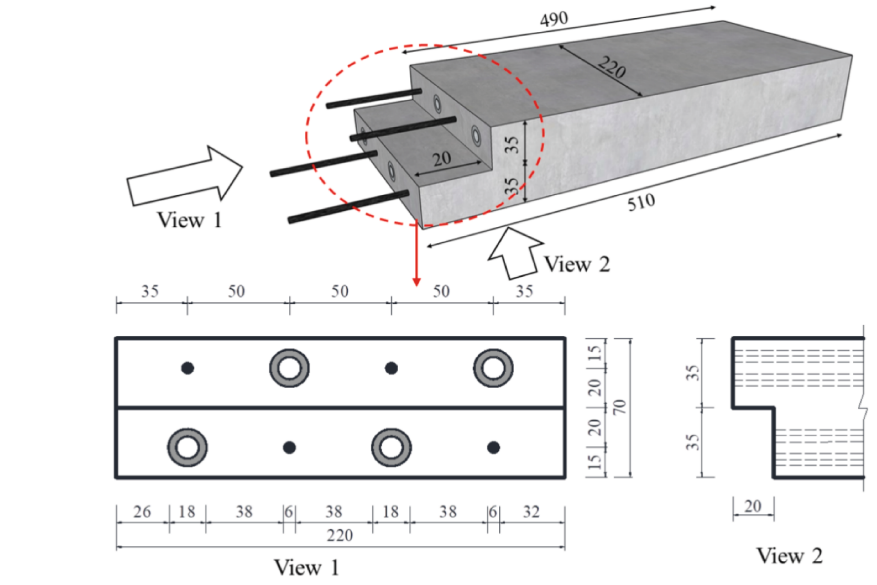

(a) Half of the plate with Mode I connection (staggered connection mode)

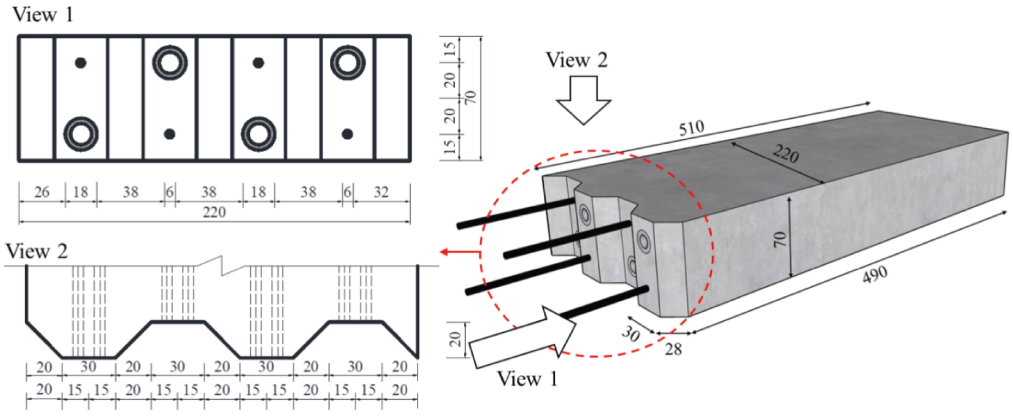

(b) Half of the plate with Mode II connection (horse tooth connection mode)

Fig. 3. Dimensions of specimens.

2. Experimental program

2.1. Specimens

A total of eight FRP bar-reinforced UHPC plates (two duplicated specimens in one group) were prepared in a way of prefabrication. The specimen details are given in Table 1. All the plate specimens with identical dimensions (length × width × thickness = 1000 mm × 220 mm × 70 mm) were designed with a connection based on carbon FRP (CFRP) bars and steel grouting sleeves. The UHPC containing PE fibers and steel fibers was also included for comparison. Two modes of connection, including a staggered connection mode and a horse tooth connection mode (Fig. 2), were proposed for the plates to explore their difference. The staggered connection mode was expected to have a good shear resistance in the thickness direction, while the horse tooth connection mode was expected to have a good shear resistance in the width direction. The test plates were reinforced with two rows of CFRP reinforcing bars with a diameter of 6 mm. The center-to-center spacing of the CFRP bars in each row was 100 mm, and a thin concrete cover thickness of 12 mm was adopted. The upper row of bars was designed to be in staggered positions to the lower row of bars for ease of connecting using steel grouting sleeves. The FRP reinforcement ratio for the plates was about 0.73 %. Steel grouting sleeves (Q345) with an outer diameter of 18 mm, a length of 180 mm and a thickness of 3 mm were adopted. The inner surface of the steel grouting sleeves was prepared to have screw threads in order to gain an enhanced bonding between the sleeves and the UHPC. The dimensions of the specimens are illustrated in Fig. 3.

As shown in Table 1, each specimen is labelled with three parts of codes connected adjacently by a character "-". "MI" and "MII" in the first part of codes denote the connection Mode I and Mode II of the UHPC plates, respectively. The second part represents the fiber type in the UHPC matrix ("SF" for steel fibers, "PE" for PE fibers), followed by a number (i.e., "1" and "2") to differentiate the nominally duplicated samples. For instance, "MI-SF-2" denotes the second composite plate specimen containing steel fibers and connected using the staggered connection mode.

2.2. Material properties

Two types of UHPC (UHPC-I and UHPC-II) were used based on the

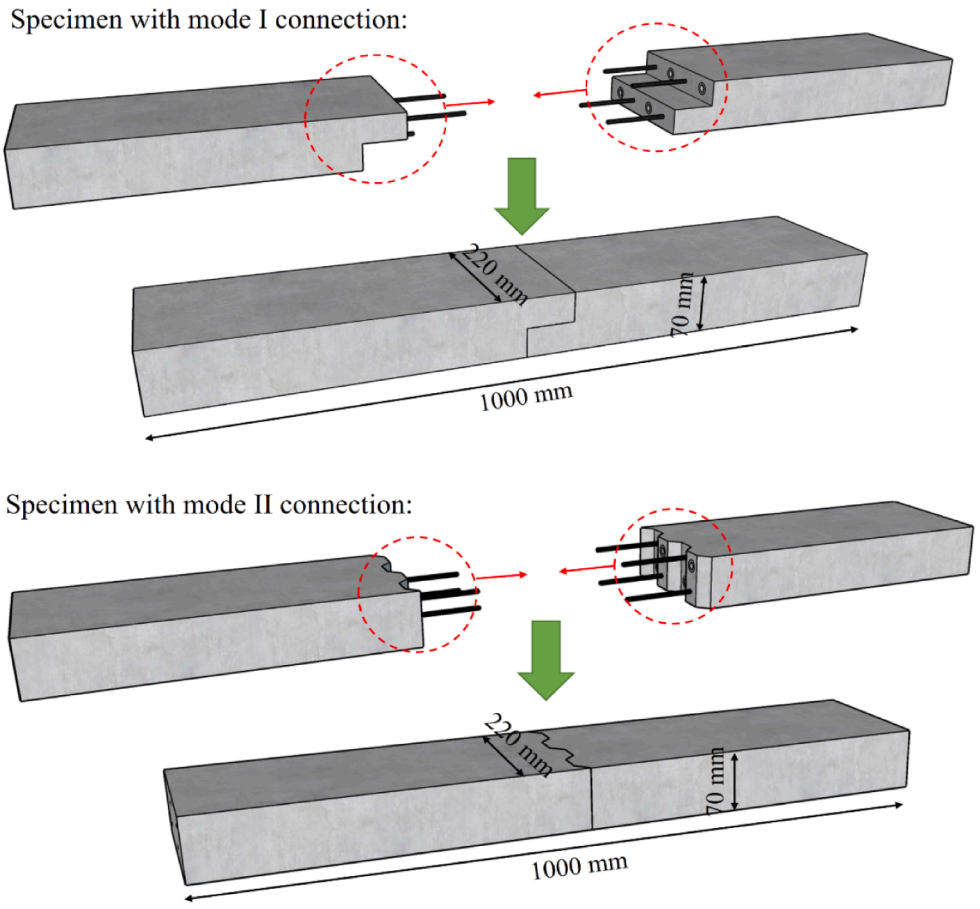

(c) Full specimen dimensions

Fig. 3. (*continued*).

Table 2
UHPC mix proportions.

Specimen	Cement (P·II 52.5R)	Quartz powder	Silica fume	Sand	GGBFS	Water	Super-plasticizer	Steel fiber	PE fiber
UHPC-I	1.00	0.37	0.25	1.10	/	0.19	0.05	1.5 % (Volume fraction)	/
UHPC-II	1.00	0.63	0.19	/	0.94	0.33	0.05	/	2 % (Volume fraction)

Note: GGBFS —— Ground granulated blast-furnace slag.

Table 3
Dimensions and mechanical properties of the short fibers used in UHPC.

Fiber type	Density (kg/m^3)	Length (mm)	Diameter (μm)	Tensile strength (MPa)	Elastic modulus (GPa)
PE fiber	970	6 &12	24	3000	100
Steel fiber	7850	13	200	>2600	200

mix proportions given in Table 2. The materials for UHPC included P•II 52.5R Portland cement, silica fume and tap water. Local river sand with an apparent density of 2652 kg/m^3 and a fineness modulus of 3.10 and quartz powder with particles sized in 20–40 mesh and 70–140 mesh (mixed in volume fraction of 1:1) were adopted as aggregate. Polycarboxylate-based superplasticizer with a solid content of 20 % was employed. Two types of fibers were used in this study, including steel fibers and PE fibers. Table 3 gives the dimensions and the material

Table 4
Compressive properties.

Specimen	Compressive strength (MPa)f'_{cc}	Elastic modulus (GPa)E_c	Ultimate compressive strain
UHPC-I-1	139.5	49.7	0.0030
UHPC-I-2	158.4	51.0	0.0033
UHPC-I-3	167.3	54.4	0.0032
Mean	155.1	51.7	0.0032
UHPC-II-1	118.6	38.4	0.0034
UHPC-II-2	123.2	42.5	0.0035
UHPC-II-3	115.1	38.1	0.0035
Mean	119.0	39.7	0.0035

Note: "UHPC-I" — UHPC cylinders with steel fibers; "UHPC-II" — UHPC cylinders with PE fibers.

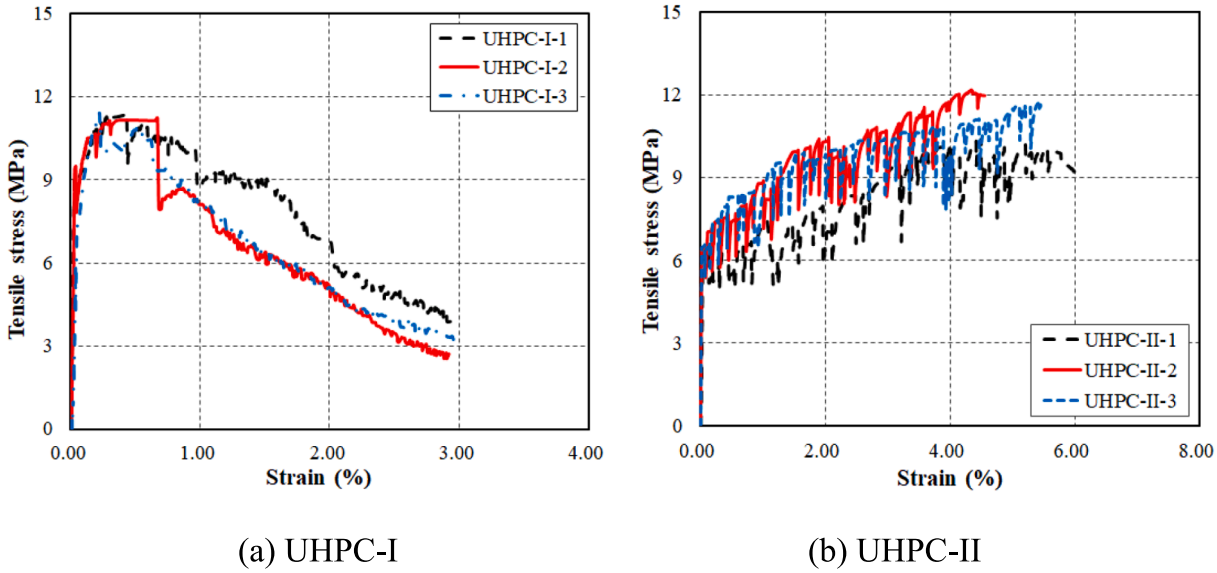

Fig. 4. Tensile stress–strain curves of UHPC dumbbell samples.

properties for each type of short fibers.

For each mix design of UHPC, three dumbbell specimens and three cylinders with a diameter of 50 mm and a height of 100 mm were prepared to investigate the UHPC's tensile and compressive material properties, according to the JSCE code [40]. Table 4 reports the compressive strength, elastic modulus and ultimate compressive strain of the UHPC cylinders. Fig. 4 shows the tensile stress–strain curves of UHPC dumbbell samples. It should be noted that the dumbbell samples had a total length of 300 mm, a thickness of 14 mm, a width of 60 mm. In the test portion, the length was 80 mm, and the width was reduced to be 30 mm. Two linear variable displacement transducers (LVDTs) were used to capture the strains in the sample, which was under direct tensile loading with a rate of 0.2 mm/min. It is evident that UHPC dumbbell samples with steel fibers exhibit a three-segment stress–strain curve with a first ascending segment, a strain-hardening segment after matrix cracking followed by a strain-softening second segment, while those with PE fibers exhibit a first ascending segment followed by a strain hardening second segment, which is in line with previous studies [14]. The clear zigzags in the UHPC-II curve (Fig. 4a) were due to unexpected movement of the holder for the LVDTs.

The CFRP bars were provided by Nanjing Fenghui Composite Mateiral Co., ltd. The average tensile strength, elastic modulus and ultimate tensile strain were 2318.5 MPa, 147.0 GPa and 1.60 % respectively based on tensile tests on CFRP bar samples according to the CSA S806 [41].

2.3. Specimen preparation

Steel plates (with staggered or horse tooth profile) were used to mould required section of connection of UHPC (Fig. 5a). For each half of the prefabricated UHPC plate specimen, steel grouting sleeves (Fig. 5b), the FRP bars and the steel plate were fixed at the edge of a timber mould when casting the UHPC (Fig. 5c and 5d). The two halves of the specimen were assembled by inserting the reserved CFRP bars into innermost of the expansive cement mortar (containing about 30 % calcium oxide) filled steel grouting sleeves (Fig. 5e). The seal between the two prefabricated parts was filled with a thin layer of epoxy resin.

2.4. Flexural test setup

For each plate, six micro strain gauges (SGs) with a gauge length of 1 mm were pasted to the FRP bars of the lower row in the longitudinal direction (see Fig. 6). The plates were tested with a clear span of 900 mm under four-point bending at a loading rate of 0.5 mm/min until a substantial deflection was reached. Three LVDTs at the mid-span and two support locations were installed to capture the deflections (see Fig. 6). Digital image correlation system was adopted to measure the deformation of the plates. During the test, digital images were captured every 1 s.

3. Test results and discussions

3.1. Failure mode

Fig. 7 shows the final failure modes of representative specimens, which demonstrates that all the specimens failed with a major flexural crack outside the connection zone (generally at the outmost section of the steel sleeves). The failure mode endorses the proposed connection modes for FRP bar-reinforced UHPC plates. In Fig. 8, the crack patterns of selected specimens (MII-SF-1 and MI-PE-1) at different loading stages are presented, indicating the majority of small cracks appeared at the loading stage of Point B (before reaching the peak load). Also, the critical cracks located outside the connection zone for both the connection modes. The above failure mode shows that the connection zone was intact (cracks with a small opening could be seen, as will be discussed in the next section) until the plates had experienced substantial deflection, demonstrating the reliability of both the proposed connection approaches.

3.2. Load-deflection curves

The load-midspan deflection curves of the test specimens are shown in Fig. 9. it can be seen that the FRP bar-reinforced UHPC plates have a three-segment load–deflection behavior (Fig. 9a). Taking specimen MII-SF-1 as illustration, the curve exhibits a first linear segment (segment a-b, Fig. 9a), a second nonlinear segment (segment b-c, Fig. 9a) with reducing tangent slope and a post-peak descending segment (segment c-d, Fig. 9a). It can be seen that there is little difference in the first segments of all the specimens. For the specimens with the UHPC-I mix (Fig. 9a), their second segments are generally identical (the difference in the peak loads is within 10 % for specimens with the UHPC-I mix) except that the peak load of MI-SF-I is larger than other three specimens. This is probably because the crack width of MI-SF-1 was smaller those of the other specimens, as can be seen in Fig. 7. It is thus believed that the connection mode has a negligible influence on the load–deflection

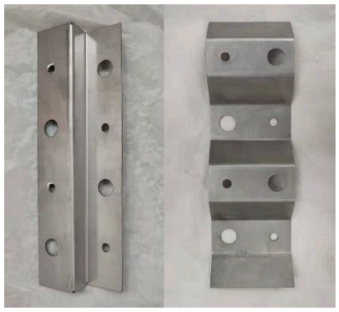

(a) Steel plates

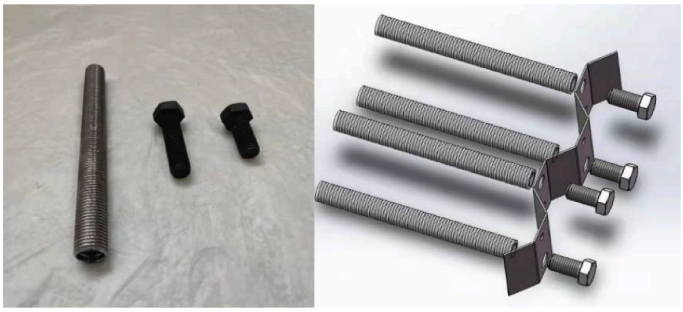

(b) Grouting sleeves

(c) Timber formwork

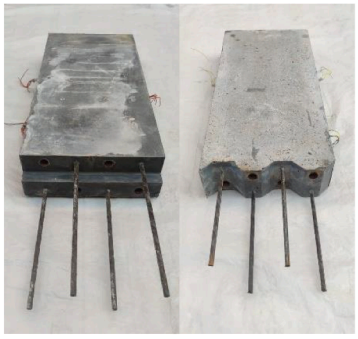

(d) FRP-UHPC plate specimens

(e) Assembling of specimens

Fig. 5. Preparation of specimens.

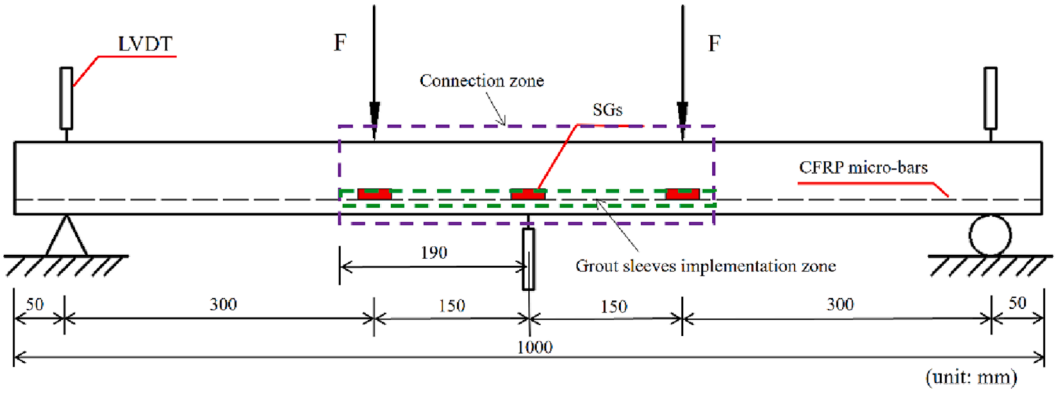

Fig. 6. Locations of SGs and LVDTs.

behavior of the connected plates with steel fibers. For specimens with PE fibers, the connection Mode II leads to a slightly larger peak load than the connection Mode I because UHPC with PE fibers had a tensile strain hardening behavior and the horse tooth connection does not have a connection surface in the longitudinal direction. Specimens with steel fibers have a post-peak descending load–deflection curves, while the applied loads at the third segment of the load–deflection curves for specimens with PE fibers remain stable, suggesting the PE fibers provide

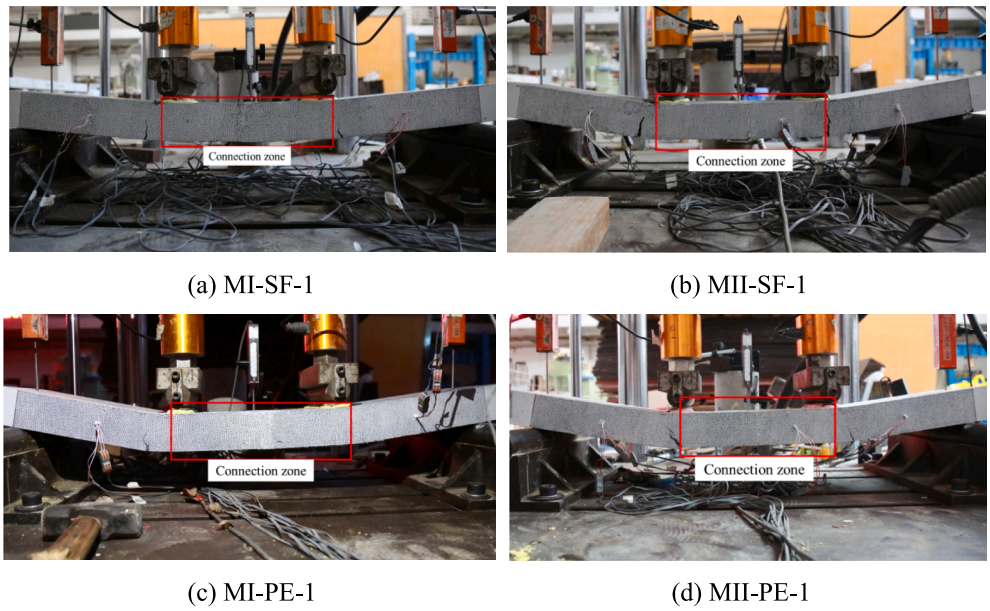

(a) MI-SF-1 (b) MII-SF-1

(c) MI-PE-1 (d) MII-PE-1

Fig. 7. Failure mode.

sufficient bridge action in resisting crack widening at this stage. Some specimens experienced progress failure (e.g., MII-SF-1) and exhibited an obvious load decline in the post-peak descending segment. This was due to the small slip (about 0.5 mm at peak load) between the CFRP bars and the UHPC matrix, as could be observed in the ends of the FRP bar-reinforced UHPC plates.

At a given tolerable deflection of 1/200 span (about 5 mm), the corresponding applied loads are about 30 kN for specimens with steel fibers, while it is about 20 kN for specimens with PE fibers. This suggests that specimens with steel fibers may have a larger usable bending capacity than specimens with PE fibers. This can also be demonstrated by comparing the load–deflection curves of specimens in Fig. 9c and 9d. The first crack load (P_{cr}), the peak load (P_{cm}), the ultimate load (P_{cu} = 0.85 P_{cm}) and corresponding deflections are summarized in Table 5. The first crack load is determined by the first curvature change point of the load deflection curve (see point 'b' in Fig. 9). The crack opening displacements at the interface of the connection at the ultimate load are summarized in Table 5. It can be seen that the crack opening displacements at the interface of the connection for the Mode I connection specimens are larger than those of the Mode II connection specimens, and most of the crack opening displacements are smaller than 0.2 mm at ultimate. The ductility coefficient (Δ_{cm}/Δ_{cr}) shows that all the connected plates exhibit an excellent ductility and the specimens with the horse tooth connection mode have a better ductility than those with the staggered connection mode. The ductility coefficients of specimens with connection Mode I are considerably large due to their very small crack deflections (see Table 5).

3.3. Load-strain curves

The FRP longitudinal strains at the mid-span and the those near the transition zone and the normal zone are plotted against the applied load in Fig. 10. It can be seen the longitudinal strains at the mid-span are smaller than those at the transition zone and the normal zone. At given tolerable deflection of 1/200 span (about 5 mm), the longitudinal strain at mid-span developed in the CFRP bars was about 2000 $\mu\varepsilon$ for all specimens. This amount of longitudinal strain is within the suggested design limit specified in the current design code (CSA S806 [41]). The strain development manners of FRP bars in SF UHPC and PE UHPC are significantly different. After the initial cracking, the strains of CFRP bars in PE UHPC plates were almost linearly proportional to the applied load, while those in SF UHPC plates obviously were nonlinearly proportional to the applied load. This is because strain localization (strain softening) occurred in SF UHPC plates. As a result, the axial strain developed in the CFRP bars in SF UHPC was about 7000 $\mu\varepsilon$ when the peak load was reached while this value was about 6000 $\mu\varepsilon$ (see Fig. 10) although the deformability of both types of members was similar at the peak loads (Fig. 9). It should be noted that the readings of strains were not available at the ultimate failure due to failure of strain gauges.

4. Theoretical analysis on flexural capacity of FRP bar Reinforced-UHPC plates

As previous studies have demonstrated that the plain section assumption is valid for FRP reinforced-UHPC plates, the flexural capacity of FRP bar reinforced-UHPC plates can be calculated based on the sectional analysis. In this study, the following assumptions are adopted: 1) the section strain distribution follows the assumption of plane section (Fig. 11 and Equation (1)); 2) the compressive stress–strain curve of UHPC shows a linear upward trend before reaching its peak stress (i.e., $\varepsilon_{u,c}$ is not larger than the compressive strain at peak stress, ε_{co}) (Fig. 11c); 3) in the equivalent stress distribution (Fig. 11c), the tensile stress of steel/PE fiber-reinforced UHPC in tensile zone after cracking is assumed to be equal to its initial cracking strength.

$$\frac{\varepsilon_{u,c}}{\varepsilon_{frp}} = \frac{x_c}{h_0 - x_c} \tag{1}$$

Therefore, the equilibrium equations at mid-span section can be expressed as follows:

$$0.5E_c\varepsilon_{u,c}x_c b = f_{t0}b(h - x_c) + A_f E_f \varepsilon_{frp} \tag{2}$$

$$M = f_{t0}(h - x_c)b\left(\frac{h - x_c}{2} + \frac{2x_c}{3}\right) + A_f E_f \varepsilon_{frp}\left(h_0 - \frac{x_c}{3}\right) \tag{3}$$

where E_c is the compressive modulus of UHPC matrix; x_c is the height of the compression zone; f_{t0} is the initial cracking strength of UHPC matrix; b and h are the width and the height of the plate, respectively; A_f, E_f and ε_{frp} are the total cross-sectional area, the elastic modulus and the rupture strain of the FRP bar. In addition, the strain efficiency factor of the FRP bar was found to be around 0.6 and thus for the specimens with strain gauge failure before FRP rupture, the rupture strain of the FRP bar was taken as 0.6 times the ultimate tensile strain of FRP bar (i.e., ε_{frp} =

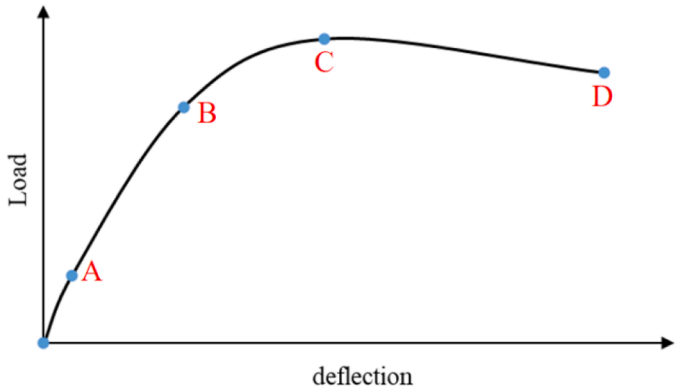

(a) Typical load-deflection curve

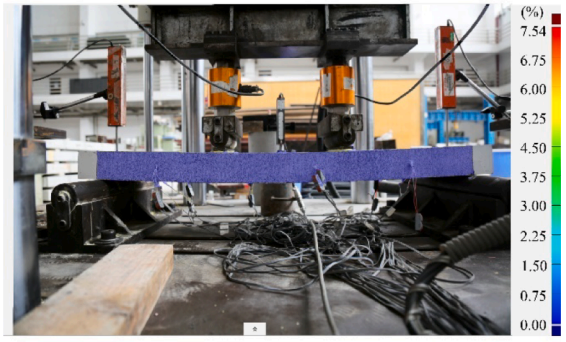

(b) MII-SF-1 (Point A)

(c) MI-PE-2 (Point A)

(d) MII-SF-1 (Point B)

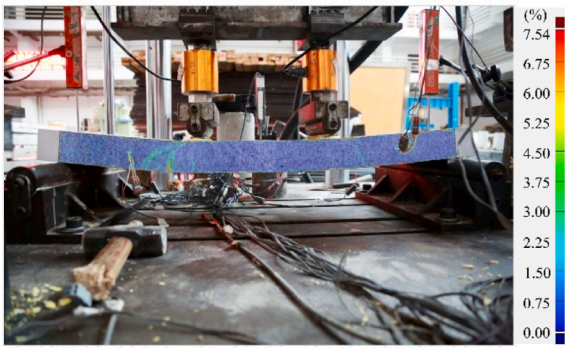

(e) MI-PE-2 (Point B)

(f) MII-SF-1 (Point C)

(g) MI-PE-2 (Point C)

Fig. 8. Deformation of specimens at different loading stages based on DIC results.

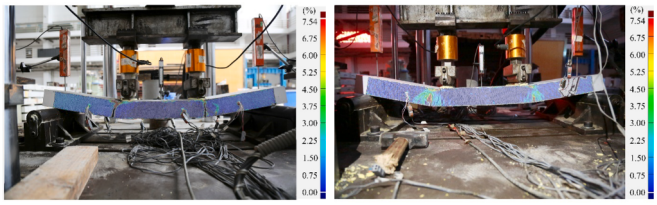

(h) MII-SF-1 (Point D) (i) MI-PE-2 (Point D)

Fig. 8. (*continued*).

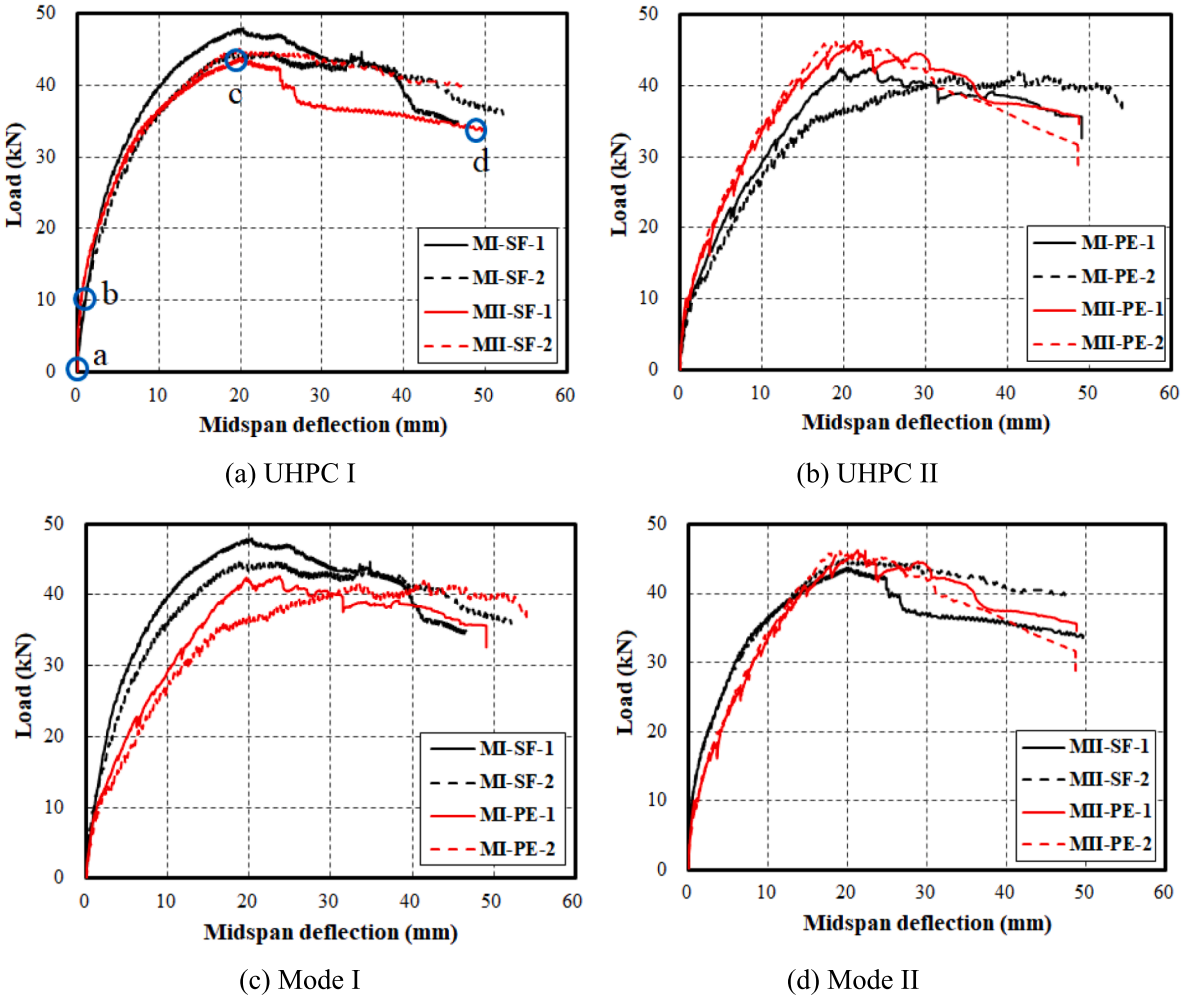

Fig. 9. Load-midspan deflection curves of the connected FRP reinforced UHPC plates.

Table 5
Summary of key test results.

Specimen	P_{cr} (kN)	Δ_{cr} (mm)	P_{cm} (kN)	Δ_{cm}(mm)	P_{cu} (kN)	Δ_{cu} (mm)	$\omega_{c,m}$ (mm)	$\omega_{c,t}$ (mm)	μ
MI-SF-1	11.8	1.20	47.8	19.95	40.6	39.38	0.15	8.48	16.6
MI-SF-2	11.7	1.23	44.2	19.67	37.6	46.41	0.14	7.54	16.0
MII-SF-1	10.0	0.42	43.8	20.07	37.2	28.60	0.08	7.62	47.8
MII-SF-2	10.6	0.54	45.1	19.86	40.2	45.10	0.12	7.52	36.8
MI-PE-1	11.3	1.69	42.4	19.64	36.1	45.89	0.11	5.48	11.6
MI-PE-2	10.6	1.85	41.3	32.89	35.1	54.01	0.11	1.70	17.8
MII-PE-1	10.0	1.00	46.0	21.30	39.1	36.19	0.00	4.11	21.3
MII-PE-2	10.6	1.19	46.3	22.02	39.2	34.21	0.00	4.84	18.5

Note: P_{cr} — The first crack load; Δ_{cr} — The deflection at the first crack load; P_{cm} — The peak load; Δ_{cm} — The deflection at the peak load; P_{cu} — The ultimate load; Δ_{cu} — The deflection at the ultimate load; $\omega_{c,m}$ — The ultimate crack opening displacement at the mid-span; $\omega_{c,t}$ — The ultimate crack opening displacement at the connection zone and the normal zone of the specimen; μ — The ductility coefficient (Δ_{cm}/Δ_{cr}).

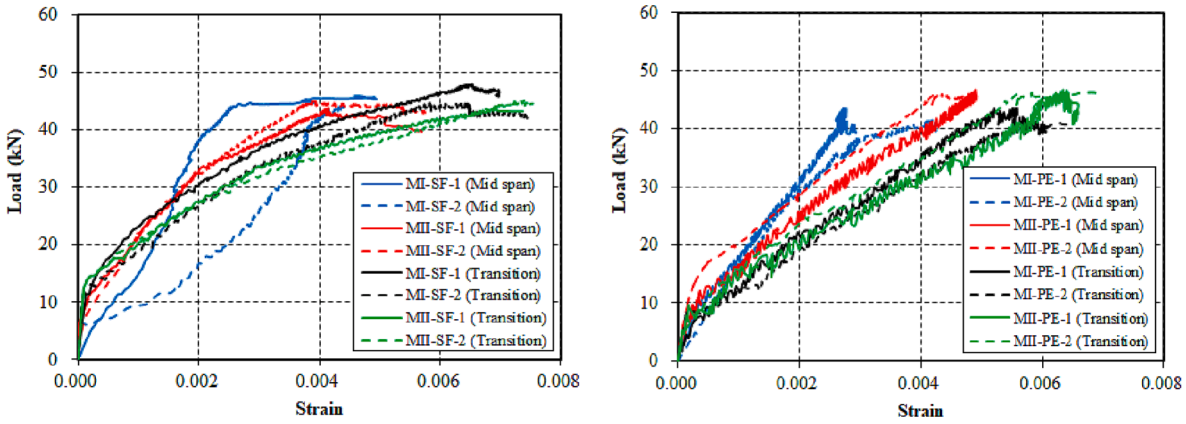

Fig. 10. Load-strain curves of test plates.

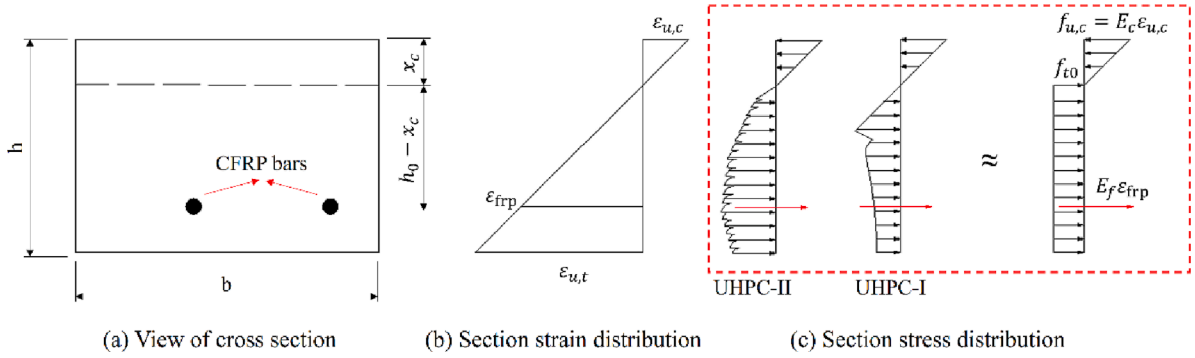

Fig. 11. Calculation of the mid-span section moment.

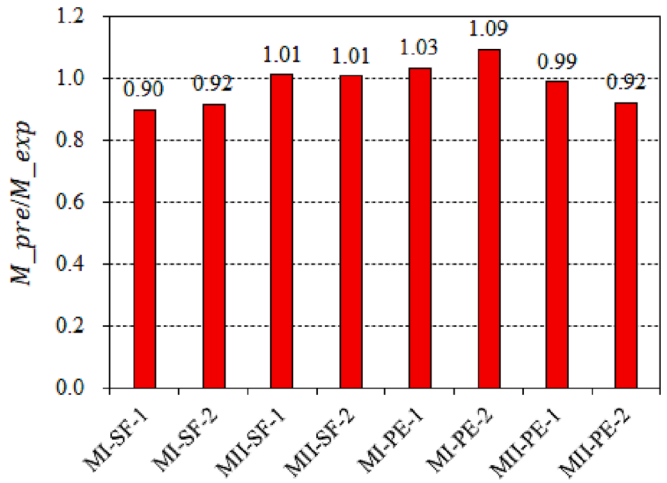

Fig. 12. Ratios between the predicted and the experimental mid-span section moment.

$0.6\varepsilon_f$). Fig. 12 shows the comparison of the predicted and experimental mid-span section moment. It can be found that most of the predicted results are in close agreement with the experimental results from the current study, demonstrating the reliability of the sectional analysis approach.

5. Conclusions

This paper has presented the development of a novel connection system for UHPC plates based on CFRP bars and steel sleeves and the investigation on flexural behavior of connected UHPC plates. The effects of the fiber type (polyethylene (PE) fibers and steel fibers) and connection mode (the staggered connection and the horse tooth connection) on the flexural behavior of FRP bar-reinforced-UHPC composite plates were explored to verify the effectiveness of the proposed connection system. The following conclusions are drawn:

1. Both the staggered and the horse tooth connections are reliable as the connected plates experienced flexural cracking failure outside the connection zone. The crack width of the UHPC plates with steel fibers at peak load was larger than that in UHPC plates with PE fibers.
2. The Mode II UHPC plates had a smaller crack width than the Mode I UHPC plates with PE fibers, implying the efficacy of the Mode II connection is better than the Mode I connection.
3. The FRP bar-reinforced UHPC plates with each mode of connection have a three-segment load–deflection behavior. The first segments of all the specimens are independent to the key parameters, and the connection mode has negligible influence on the load–deflection behavior of the connected plates with steel fibers. For plates with PE fibers, the horse tooth mode leads to a slightly enhanced peak load than that of the staggered connection mode.
4. The connected plates exhibit an excellent ductility, and the specimens with the horse tooth connection mode have a better ductility than those with the staggered connection mode.
5. The longitudinal strains developed in the CFRP bars at the given tolerable deflection of 1/200 is about 2000 με, which is within the suggested design limit strain specified in the current design code.

CRediT authorship contribution statement

Jun-Jie Zeng: Conceptualization, Funding acquisition, Supervision, Methodology, Writing – original draft, Writing – review & editing. **Shu-**

Peng Chen: Investigation, Data curation. **Peng Feng:** Writing – review & editing. **Yan Zhuge:** Supervision, Writing – review & editing. **Kai-Di Peng:** Investigation, Data curation. **Jian-Guo Dai:** Supervision, Funding acquisition, Writing – review & editing. **Tian-Hui Fan:** Writing – review & editing.

Declaration of Competing Interest

The authors declare that they have no known competing financial interests or personal relationships that could have appeared to influence the work reported in this paper.

Data availability

Data will be made available on request.

Acknowledgements

The authors acknowledge the financial support received from the Natural Science Foundation of Guangdong Province (No. 2019A1515011637, 2021A0505060008), the Hong Kong Innovation and Technology Fund (No. ITS/077/18FX).

References

[1] Shi C, Wu Z, Xiao J, Wang D, Huang Z, Fang Z. A review on ultra high performance concrete: part I. raw materials and mixture design. Constr Build Mater 2015;101:741–51.
[2] Xie T, Fang C, Ali MNS, Visintin P. Characterizations of autogenous and drying shrinkage of ultra-high performance concrete (UHPC): an experimental study. Cem Concr Compos 2018;91:156–73.
[3] Yoo DY, Banthia N. Mechanical properties of ultra-high-performance fiber-reinforced concrete: a review. Cem Concr Compos 2016;73:267–80.
[4] Li WG, Huang ZY, Hu GQ, Duan WH, Shah SP. Early-age shrinkage development of ultra-high-performance concrete under heat curing treatment. Constr Build Mater 2017;131:767–74.
[5] Sawicki B, Brühwiler E, Denarié E. Inverse analysis of R-UHPFRC beams to determine the flexural response under service loading and at ultimate resistance. J Struct Eng ASCE 2022;148(2):04021260.
[6] Bastien-Masse M, Denarié E, Brühwiler E. Effect of fiber orientation on the in-plane tensile response of UHPFRC reinforcement layers. Cement Concrete Compos 2016;67:111–25.
[7] Teng JG, Xiang Y, Yu T, Fang Z. Development and mechanical behaviour of ultra-high-performance seawater sea-sand concrete. Adv Struct Eng 2019;22(14):3100–20.
[8] Zeng JJ, Pan BZ, Fan TH, Zhuge Y, Liu F, Li LJ. Shear behavior of FRP-UHPC tubular beams. Compos Struct 2023;307:116576.
[9] Miletić M, Kumar LM, Arns JY, Agarwal A, Foster SJ, Arns C, et al. Gradient-based fibre detection method on 3D micro-CT tomographic image for defining fibre orientation bias in ultra-high-performance concrete. Cem and Concr Res 2020;129:105962.
[10] Zhou PZ. Feng P.Unified analysis for tailorable multi-scale fiber reinforced cementitious composites in tension. Compos Part B: Eng 2023;254:110586.
[11] Zhu ZF, Wang WW, Hui YX, Hu SW, Men GY, Tian J, et al. Mechanical behavior of concrete columns confined with CFRP grid-reinforced engineered cementitious composites. J Compos Constr 2022;26(1):04021060.
[12] Meng W, Khayat KH, Bao Y. Flexural behaviors of fiber-reinforced polymer fabric reinforced ultra-high-performance concrete panels. Cem Concr Compos 2018;93:43–53.
[13] Ye YY, Smith ST, Zeng JJ, Zhuge Y, Quach WM. Novel ultra-high-performance concrete composite plates reinforced with FRP grid: Development and mechanical behaviour. Compos Struct 2021;268:114033.
[14] Zeng JJ, Feng P, Zhuge Y, Dai JG. Development and behavior of novel FRP-UHPC tubular members. Eng Struct 2022;266:114540.
[15] Pan BZ, Liu F, Zhuge Y, Zeng JJ, Liao JJ. ECC/UHPFRCC with and without FRP reinforcement for structural strengthening/repairing: a state-of-the-art review. Constr Build Mater 2022;315:125824.
[16] Jiang JF, Jiang C, Li BB, Feng P. Bond behavior of basalt textile meshes in ultra-high ductility cementitious composites. Compos Part B Eng 2019;174:107022.
[17] Gonzalez-Libreros JH, Sneed LH, D'Antino T, Pellegrino C. Behavior of RC beams strengthened in shear with FRP and FRCM composites. Eng Struct 2017;150:830–42.
[18] De Luca A, Nardone F, Matta F, Nanni A, Lignola G, Prota A. Structural evaluation of full-scale FRP-confined reinforced concrete columns. J Compos Constr, ASCE 2011;15(1):112–23.
[19] Zeng JJ, Lin G, Teng JG, Li LJ. Behavior of large-scale FRP-confined rectangular RC columns under axial compression. Eng Struct 2018;174:629–45.
[20] Liao JJ, Yang KY, Zeng JJ, Quach WM, Ye YY, Zhang LH. Compressive behavior of FRP-confined ultra-high performance concrete (UHPC) in circular columns. Eng Struct 2021;249:113246.
[21] Gooranorimi O, Nanni A. GFRP reinforcement in concrete after 15 years of service. J Compos Constr, ASCE 2017;21(5).
[22] Zhou JK, Zeng JJ, Liang QJ, Dai HS, Fan TH. Compressive behavior of PET FRP-confined concrete encased CFST columns. J Constr Steel Res 2023;202:107732.
[23] Zeng JJ, Ye YY, Liu WT, Zhuge Y, Liu Y, Yue YQ. Behaviour of FRP spiral-confined concrete and contribution of FRP longitudinal bars in FRP-RC columns under axial compression. Eng Struct 2023;281:115747.
[24] Zhang YR, Wei Y, Bai JW, Wu G, Dong ZQ. A novel seawater and sea sand concrete filled FRP-carbon steel composite tube column: concept and behavior. Compos Struct 2020;246(8):112421.
[25] Zhu DH, Zhong GQ, Zeng JJ, Liao JJ. Behavior and model evaluation of large-rupture-strain (LRS) FRP-confined concrete-encased high-strength steel columns under axial compression. Thin-Walled Struct 2023;183:110367.
[26] Meng, W., K.H. Khayat. "Experimental and numerical studies on flexural behavior of ultrahigh-performance concrete panels reinforced with embedded glass fiber-reinforced polymer grids." *Transp. Res. Rec.* 2592 (1): 38–44.
[27] Zeng JJ, Zeng WB, Yu-Yi Ye JJ, Liao Y, Zhuge THF. Flexural behavior of FRP grid reinforced ultra-high-performance concrete composite plates with different types of fibers. Eng Struct 2022;272:115020.
[28] Dong ZQ, Sun Y, Wu G, Zhu H, Zhao XL, Wei Y, et al. Flexural behavior of seawater sea-sand concrete beams reinforced with BFRP bars/grids and BFRP-wrapped steel tubes. Compos Struct 2021;268:113956.
[29] Lin G, Zeng JJ, Liang SD, Liao JJ, Zhuge Y. Seismic behavior of novel GFRP bar reinforced concrete beam-column joints internally reinforced with an FRP tube. Eng Struct 2022;273:115100.
[30] Hadi MNS, Karim H, Sheikh MN. Experimental investigations on circular concrete columns reinforced with GFRP Bars and helices under different loading conditions. J Compos Constr 2016;20(4):04016009.
[31] Xue W, Peng F, Fang Z. Behavior and design of slender rectangular concrete columns longitudinally reinforced with fiber-reinforced polymer bars. ACI Struct J 2018;115(2):311–22.
[32] Zeng JJ, Liao JJ, Zhuge Y, Guo YC, Zhou JK, Huang ZH, et al. Bond behavior between GFRP bars and seawater sea-sand fiber-reinforced ultra-high strength concrete. Eng Struct 2022;254:113787.
[33] Hassanli R, Vincent T, Manalo A, Smith ST, Gholampour A, Gravina R. Large-scale experimental study on pocket connections in GFRP-reinforced precast concrete frames. Structures 2021;34:523–41.
[34] ACI 440.1 R. Guide for the design and construction of structural concrete reinforced with FRP bars (ACI 440.1 R-15).
[35] Association CS. CSA-S806-02. ON, Canada: Design and Construction of Building Components with Fibre-Reinforced Polymers. Toronto; 2002.
[36] C.S. Association Canadian highway bridge design code (CAN/CSA S6–06), Ontario, Toronto (2006).
[37] Zhou JF, Stümpel M, Kang CJ, Marx S. Lap-spliced connections of steel and FRP bars in reinforced flexure concrete structures. Eng Struct 2022;263:114409.
[38] Zhang L, Bai Y, Qi Y, Fang H, Wu BS. Post-fire mechanical performance of modular GFRP multicellular slabs with prefabricated fire resistant panels. Compos Part B Eng 2018;143:55–67.
[39] Zhang Z, Bai Y, He X, Jin L, Zhu L. Cyclic performance of bonded sleeve beam-column connections for FRP tubular sections. Compos Part B Eng 2018;142:171–82.
[40] JSCE. Recommendations for Design and Construction of High Performance Fiber Reinforced Cement Composites with Multiple Fine Cracks (HPFRCC). Concrete Eng Series No 2008;82:2008.
[41] CSA s806,. Design and construction of building components with fiber-reinforced polymers. Ontario, Canada: Canadian Standard Association; 2012.